

## Supplemental materials and methods

### Evaluation of the effect of the rate of FRET change of IRIS-1 upon IP<sub>3</sub> binding

The change of the intensity of Venus fluorescence ( $525 \pm 20$  nm) of IRIS-1 excited at  $440 \pm 20$  nm after the addition of various concentrations of IP<sub>3</sub> was monitored using a stopped-flow fluorescence spectrometry (Fig. S2 A). We found a good fit between all of the traces except the control experiments (without IP<sub>3</sub>) and a double exponential function (Fig. S2 A). Because the time constant of the slow component (1.2–16.7 s) was almost constant irrespective of [IP<sub>3</sub>] applied (unpublished data) and was close to the time constant (2.9 s) of a single exponential function fitted to the fluorescent intensity change observed without the addition of IP<sub>3</sub> (Fig. S2 A), the fast component alone was used for the evaluation of the reaction rate of IRIS-1. Fig. S2 B shows the relationship between the inverse time constants of the fast component and [IP<sub>3</sub>] applied. The inverse time constant was changed depending on [IP<sub>3</sub>] in a nonlinear hyperbolic manner, indicating that the IP<sub>3</sub> binding is not a rate-limiting step for the FRET change of IRIS-1 and that conformational changes of the IRIS-1 molecule may be involved in the reaction. We therefore applied the following model for the evaluation of the reaction mechanism of IRIS-1:



where [IP<sub>3</sub>] is the concentration of IP<sub>3</sub>, [IRIS] is the concentration of IP<sub>3</sub> unbound IRIS-1 with high FRET efficiency, [IP<sub>3</sub>·IRIS] is the concentration of IP<sub>3</sub> bound IRIS-1 with high FRET efficiency, [IP<sub>3</sub>·IRIS\*] is the concentration of IP<sub>3</sub> bound IRIS-1 with low FRET efficiency,  $k_{\text{on}}$  is the association rate constant,  $k_{\text{off}}$  is the dissociation rate constant,  $k_f$  is the rate constant of the forward conformational change, and  $k_r$  is the rate constant of the reverse conformational change. In this model, a conformational change accompanied with FRET change occurs after IP<sub>3</sub> binding, and the relationship between the fraction of [IP<sub>3</sub>·IRIS\*] and [IP<sub>3</sub>] at equilibrium is described as follows:

$$\frac{[\text{IP}_3 \cdot \text{IRIS}^*]}{[\text{IRIS}]_{\text{total}}} = \frac{1}{K_1 K_2 / [\text{IP}_3] + K_2 + 1} \quad (2)$$

$$[\text{IRIS}]_{\text{total}} = [\text{IRIS}] + [\text{IP}_3 \cdot \text{IRIS}] + [\text{IP}_3 \cdot \text{IRIS}^*] \quad (3),$$

where [IRIS]<sub>total</sub> is the total concentration of IRIS-1,  $K_1$  is  $k_{\text{off}}/k_{\text{on}}$  (the equilibrium constant of the interaction between IP<sub>3</sub> and IRIS-1), and  $K_2$  is  $k_r/k_f$  (the equilibrium constant of the conformational change of IP<sub>3</sub> bound IRIS-1). The equation provides reasonable fits with the parameters,  $K_1 = 7.26 \times 10^{-5}$  (M) and  $K_2 = 0.00269$ , and the experimental data measured at equilibrium (Fig. S2 C, solid line). We then tried to find the rate constants that fit with the apparent inverse time constants observed (Fig. S2 B) in the following equations:

$$\frac{d[\text{IP}_3 \cdot \text{IRIS}^*]}{dt} = k_f [\text{IP}_3 \cdot \text{IRIS}] - k_r [\text{IP}_3 \cdot \text{IRIS}^*] \quad (4),$$

$$\frac{d[\text{IP}_3 \cdot \text{IRIS}]}{dt} = k_{\text{on}} [\text{IP}_3][\text{IRIS}] - k_{\text{off}} [\text{IP}_3 \cdot \text{IRIS}] - k_f [\text{IP}_3 \cdot \text{IRIS}] + k_r [\text{IP}_3 \cdot \text{IRIS}^*] \quad (5),$$

$$\frac{d[\text{IP}_3]}{dt} = -k_{\text{on}} [\text{IP}_3][\text{IRIS}] + k_{\text{off}} [\text{IP}_3 \cdot \text{IRIS}] \quad (6), \text{ and}$$

$$\frac{d[\text{IRIS}]}{dt} = k_{\text{on}} [\text{IP}_3][\text{IRIS}] - k_{\text{off}} [\text{IP}_3 \cdot \text{IRIS}] \quad (7).$$

However, we did not find the parameters that satisfy the data shown in both Fig. S2 B and C because the estimated value of the equilibrium binding constant,  $K_1$ , from the data shown in Fig. S2 C is too high when it is compared with the apparent IP<sub>3</sub> sensitivity of the inverse time constants of changes in the Venus fluorescence ( $\text{EC}_{50} < 1 \times 10^{-7}$  M; Fig. S2 B). We therefore used the other model,

**Figure S1. Effects of PLC inhibitors on emission changes of IRIS-1 and evaluation of IRIS-1 signals observed in living HeLa cells.**

(A and B) Cells were pretreated with 10  $\mu\text{M}$  of PLC inhibitor U73122 (A) or its inactive analog U73343 (B) for 5 min and then with 10  $\mu\text{M}$  of histamine. Three different color plots represent data from three cells in the same viewing field. (C) Relationship between IRIS-1 signals and  $[\text{IP}_3]$  in permeabilized HeLa cells. Cells were permeabilized with 60  $\mu\text{M}$  -escin for 3 min, and bath solutions containing various concentrations of  $\text{IP}_3$  were perfused at a flow rate of 4 ml/min. Steady-state values of IRIS-1 were plotted. Error bars correspond to the standard deviation of at least six measurements. (D)  $\text{IP}_3$  sensitivity of IRIS-1 (open circles) and IRIS-1.2 (closed circles) in COS-7 lysates. The emission change of IRIS-1.2 exhibits an  $\text{IP}_3$  sensitivity with a  $K_d$  value of 4.0  $\mu\text{M}$ . Error bars correspond to the standard deviation ( $n = 3$ ). (E and F) Cells expressing mGluR5a were stimulated with 100  $\mu\text{M}$  of glutamate (horizontal bars). Signals of IRIS-1.2 (E) and Indo-1 (F) are shown. Images were acquired every 4 s. Similar results were observed in 8 out of 25 cells.

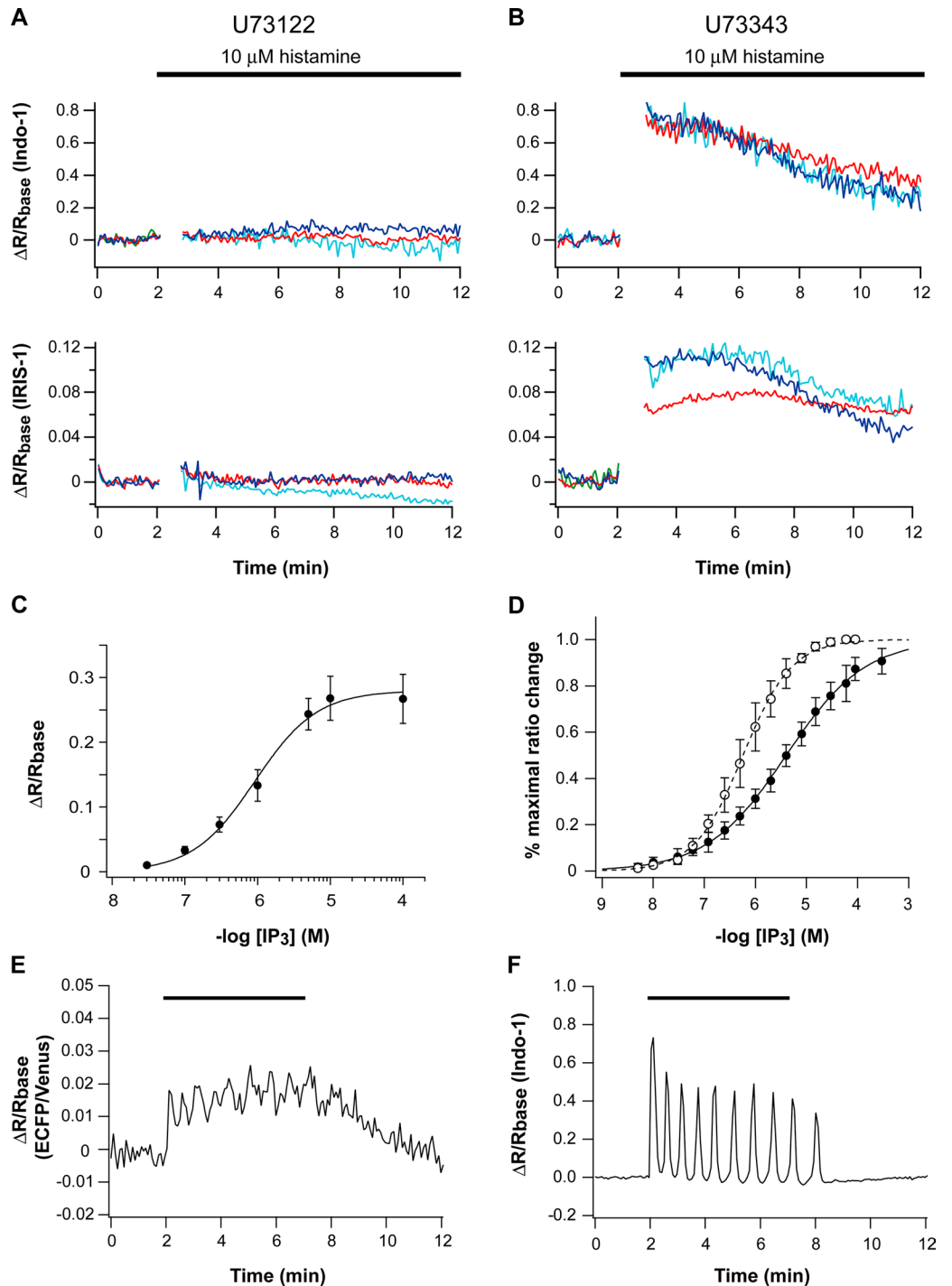


**Table S1. Numbers of cells that showed  $[\text{IP}_3]$  rises preceding  $[\text{Ca}^{2+}]$  increases and the average intervals between the onset of  $[\text{IP}_3]$  rises and the onset of  $[\text{Ca}^{2+}]$  rises**

Spike number	Cell number	Interval s
2	31 (33)	3.59 $\pm$ 2.89
3	20 (24)	2.94 $\pm$ 3.08
4	14 (19)	1.56 $\pm$ 2.44
5	13 (16)	1.96 $\pm$ 2.43
6	9 (13)	1.18 $\pm$ 2.86
7	8 (10)	1.92 $\pm$ 2.08
8	7 (9)	1.47 $\pm$ 2.41

Total numbers of cell analyzed are shown in parenthesis. Intervals are shown as mean  $\pm$  SD. Positive values indicate  $[\text{IP}_3]$  rises preceding  $[\text{Ca}^{2+}]$  rises.

Figure S2. **The rate of reaction of IRIS-1.** (A) Kinetics of Venus fluorescence intensity of IRIS-1 after the rapid mixing of 10  $\mu\text{M}$  (dark blue), 10 nM (light blue), and 0  $\text{IP}_3$  (red).  $\text{IP}_3$  was added at time 0. Double-exponential functions and a single-exponential function are shown as red smooth lines and a blue smooth line, respectively. (B) Relationship between the inverse time constant of the fast component of Venus fluorescence changes of IRIS-1 and  $[\text{IP}_3]$ . The data were obtained from three independent experiments. Error bars correspond to the standard deviation. (C) Relationship between equilibrium FRET changes of IRIS-1 and  $[\text{IP}_3]$ . The data were obtained from three independent experiments. Error bars correspond to the standard deviation. (D) Changes in the fraction of IRIS-1 with a low FRET efficiency (IRIS\* and  $\text{IP}_3$ -IRIS\*) in response to addition of a 1-s  $\text{IP}_3$  pulse (horizontal bar). Various concentrations of  $\text{IP}_3$  were used to calculate the fractional change, and all the calculated traces (0.2, 0.4, 0.8, 1.6, 3.2, 6.4, and 12.8  $\mu\text{M}$   $\text{IP}_3$ , from bottom to top) were superimposed. Basal  $[\text{IP}_3]$  was 40 nM. For more details, see the supplemental Materials and methods.

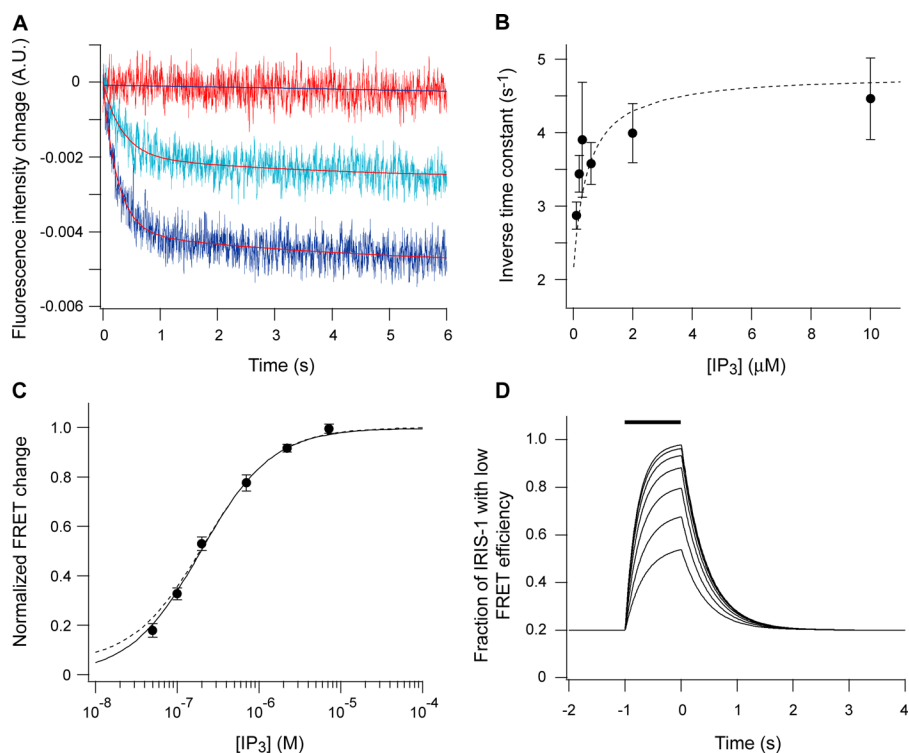


Table S2. Parameters used to calculate  $\text{IP}_3$  and  $\text{Ca}^{2+}$  dynamics

Parameter	Value		Description
	Fig. S3 (A and B)	Fig. S3 (C and D)	
$c_1$	0.185	0.185	(ER vol)/(cytosolic vol)
$v_1$	$6 \text{ s}^{-1}$	$6 \text{ s}^{-1}$	Max $\text{Ca}^{2+}$ channel flux
$v_2$	$0.11 \text{ s}^{-1}$	$0.11 \text{ s}^{-1}$	$\text{Ca}^{2+}$ leak flux constant
$v_3$	$0.9 \mu\text{M}^{-1} \text{ s}^{-1}$	$0.9 \mu\text{M}^{-1} \text{ s}^{-1}$	Max $\text{Ca}^{2+}$ uptake
$v_4$	$2.8 \text{ s}^{-1}$	$0.046 \text{ s}^{-1}$	Max $\text{IP}_3$ production rate
$k_3$	$0.1 \mu\text{M}$	$0.1 \mu\text{M}$	Activation constant for $\text{Ca}^{2+}$ pump
$k_4$	$1.1 \mu\text{M}$	$2 \mu\text{M}$	Dissociation constant for $\text{Ca}^{2+}$ stimulation of $\text{IP}_3$ production
	0.97	1	A factor for $\text{Ca}^{2+}$ dependency of $\text{IP}_3$ production
R	(0)	0.4	The fractional activation of the cell-surface receptor
$I_r$	$1 \text{ s}^{-1}$	$0.03 \text{ s}^{-1}$	Rate constant for loss of $\text{IP}_3$

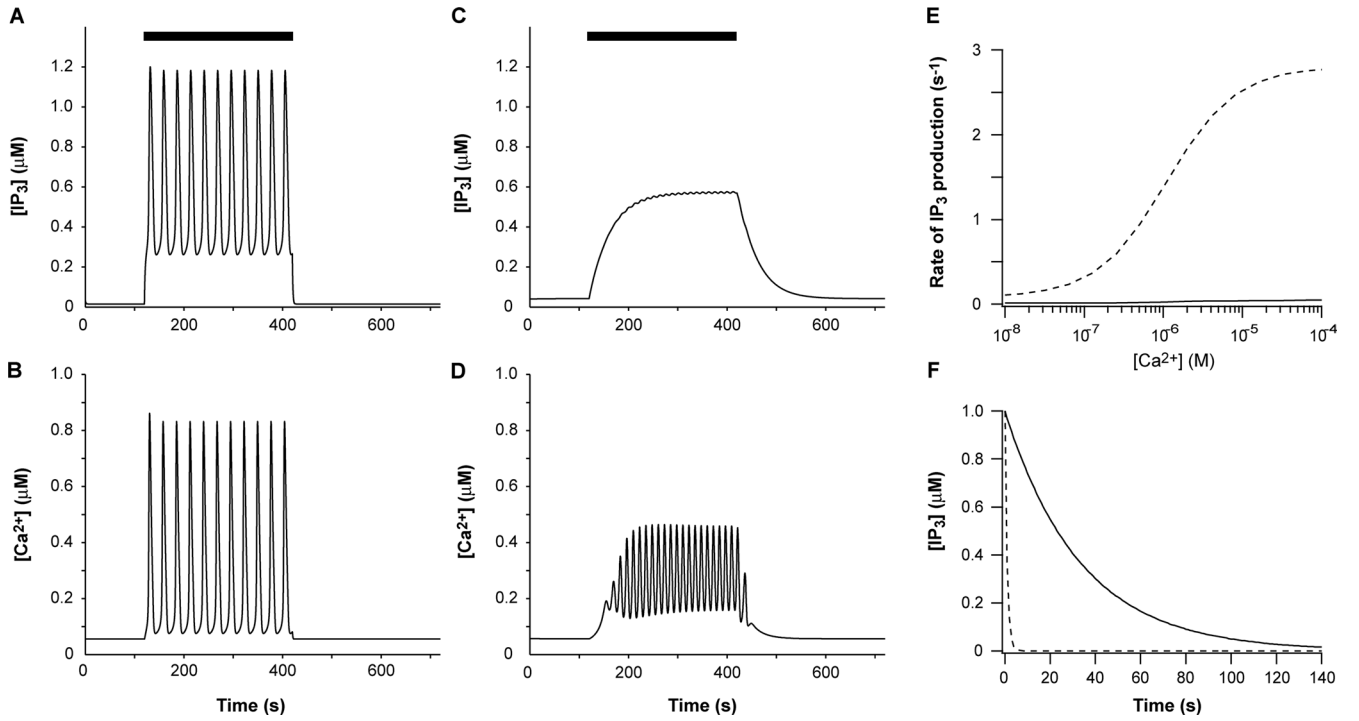


Figure S3. **Simulation of  $IP_3$  and  $Ca^{2+}$  dynamics.**  $IP_3$  and  $Ca^{2+}$  dynamics were calculated using the following model:

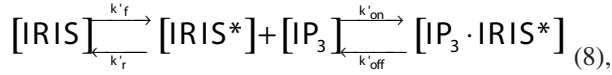
$$\frac{d[Ca^{2+}]_i}{dt} = J_1 - J_2 \quad (14)$$

$$J_1 = c_1 (v_1 x_{110}^3 + v_2) ([Ca^{2+}]_{ER} - [Ca^{2+}]_i) \quad (15)$$

$$J_2 = \frac{v_3 [Ca^{2+}]_i^2}{[Ca^{2+}]_i^2 + k_3^2} \quad (16)$$

$$\frac{d[IP_3]}{dt} = v_4 \left( 1 - \frac{\alpha k_4}{[Ca^{2+}]_i + k_4} \frac{1}{1+R} \right) - I_r [IP_3] \quad (17),$$

where  $[Ca^{2+}]_i$  is the cytosolic free  $Ca^{2+}$  concentration,  $[Ca^{2+}]_{ER}$  is the ER luminal free  $Ca^{2+}$  concentration,  $J_1$  is the outward flux of  $Ca^{2+}$ ,  $J_2$  is the inward flux, and  $x_{110}$  is the fraction of  $IP_3R$  subunits activated by both  $IP_3$  and  $Ca^{2+}$  but not yet inactivated by  $Ca^{2+}$  (De Young and Keizer, 1992). The denomination of all parameters is shown in Table S2. (A and B) Solutions using the parameters originally described in De Young and Keizer (1992). (C and D) Solutions using the parameters that produce slow  $IP_3$  metabolism. Stimulus-induced  $IP_3$  synthesis was turned on during the period shown by the horizontal bars (A–D). (E) The rates of  $IP_3$  production used in A and B (broken line) and in C and D (solid line) are shown. (F) The rates of  $IP_3$  degradation used in A and B (broken line) and in C and D (solid line) are shown.



where  $[\text{IRIS}^*]$  is the concentration of  $\text{IP}_3$  unbound IRIS-1 with a low FRET efficiency,  $k'_f$  is the rate constant of forward conformational change,  $k'_r$  is the reverse conformational change,  $k'_{\text{on}}$  is the association rate constant, and  $k'_{\text{off}}$  is the dissociation rate constant. In this model, there are two conformations of IRIS-1 with different FRET efficiencies (IRIS and  $\text{IRIS}^*$ ), and only  $\text{IRIS}^*$  is able to bind to  $\text{IP}_3$ .  $\text{IP}_3$  binding itself does not induce FRET efficiency change of IRIS-1. In this model, the relationship between the fraction of the low FRET efficiency forms ( $\text{IRIS}^*$  and  $\text{IP}_3 \cdot \text{IRIS}^*$ ) and  $[\text{IP}_3]$  at equilibrium is

$$\frac{[\text{IRIS}^*] + [\text{IP}_3 \cdot \text{IRIS}^*]}{[\text{IRIS}]_{\text{total}}} = \frac{1}{(K'_2 + 1)K'_1/[\text{IP}_3] + 1} + \frac{1}{K'_2 + [\text{IP}_3]/K'_1 + 1} \quad (9),$$

where  $K'_1 = k'_{\text{off}}/k'_{\text{on}}$  and  $K'_2 = k'_r/k'_f$ . The changes of the concentration of each form are described in the following equations:

$$\frac{d[\text{IRIS}]}{dt} = k'_r [\text{IRIS}^*] - k'_f [\text{IRIS}] \quad (10),$$

$$\frac{d[\text{IRIS}^*]}{dt} = -k'_r [\text{IRIS}^*] + k'_f [\text{IRIS}] - k'_{\text{on}} [\text{IP}_3][\text{IRIS}^*] + k'_{\text{off}} [\text{IP}_3 \cdot \text{IRIS}^*] \quad (11),$$

$$\frac{d[\text{IP}_3]}{dt} = -k'_{\text{on}} [\text{IP}_3][\text{IRIS}^*] + k'_{\text{off}} [\text{IP}_3 \cdot \text{IRIS}^*] \quad (12), \text{ and}$$

$$\frac{d[\text{IP}_3 \cdot \text{IRIS}^*]}{dt} = k'_{\text{on}} [\text{IP}_3][\text{IRIS}^*] - k'_{\text{off}} [\text{IP}_3 \cdot \text{IRIS}^*] \quad (13).$$

We found that when  $[\text{IRIS}]_{\text{total}} = 2.5 \text{ nM}$ , equations 9–13 provide good fits with the parameters  $k'_f = 4.8 \text{ (s}^{-1}\text{)}$ ,  $k'_r = 96 \text{ (s}^{-1}\text{)}$ ,  $k'_{\text{on}} = 2.1 \times 10^8 \text{ (M}^{-1} \text{ s}^{-1}\text{)}$ , and  $k'_{\text{off}} = 2.1 \text{ (s}^{-1}\text{)}$  and both the kinetic data (Fig. S2 B, broken line) and the equilibrium data (Fig. S2 C, broken line). The equilibrium constants,  $K'_1$  and  $K'_2$ , are  $1 \times 10^{-8} \text{ (M)}$  and 20, respectively. We calculated the change of the fraction of the low FRET efficiency forms ( $\text{IRIS}^*$  and  $\text{IP}_3 \cdot \text{IRIS}^*$ ) by the equations 10, 11, and 13 with the above parameters in response to the addition of a 1-s  $\text{IP}_3$  pulse and found that IRIS-1 signals return to their basal level within  $\sim 3 \text{ s}$  after the termination of  $\text{IP}_3$  pulses (Fig. S2 D).

## References

De Young, G.W., and J. Keizer. 1992. A single-pool inositol 1,4,5-trisphosphate-receptor-based model for agonist-stimulated oscillations in  $\text{Ca}^{2+}$  concentration. *Proc. Nat. Acad. Sci. USA.* 89:9895–9899.